


A chemical link between methylamine and methylene imine and implications for interstellar glycine formation

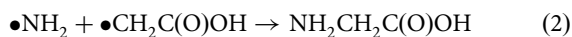
Prasad Ramesh Joshi¹ & Yuan-Pern Lee ^{1,2,3}✉

Methylamine CH_3NH_2 is considered to be an important precursor of interstellar amino acid because hydrogen abstraction might lead to the aminomethyl radical $\bullet\text{CH}_2\text{NH}_2$ that can react with $\bullet\text{HOCO}$ to form glycine, but direct evidence of the formation and spectral identification of $\bullet\text{CH}_2\text{NH}_2$ remains unreported. We performed the reaction $\text{H} + \text{CH}_3\text{NH}_2$ in solid $p\text{-H}_2$ at 3.2 K and observed IR spectra of $\bullet\text{CH}_2\text{NH}_2$ and CH_2NH upon irradiation and when the matrix was maintained in darkness. Previously unidentified IR spectrum of $\bullet\text{CH}_2\text{NH}_2$ clearly indicates that $\bullet\text{CH}_2\text{NH}_2$ can be formed from the reaction $\text{H} + \text{CH}_3\text{NH}_2$ in dark interstellar clouds. The observed dual-cycle mechanism containing two consecutive H-abstraction and two H-addition steps chemically connects CH_3NH_2 and CH_2NH in interstellar media and explains their quasi-equilibrium. Experiments on CD_3NH_2 produced CD_2HNNH_2 , in addition to $\bullet\text{CD}_2\text{NH}_2$ and CD_2NH , confirming the occurrence of H addition to $\bullet\text{CD}_2\text{NH}_2$.

¹Department of Applied Chemistry and Institute of Molecular Science, National Yang Ming Chiao Tung University, Hsinchu, Taiwan. ²Center for Emergent Functional Matter Science, National Yang Ming Chiao Tung University, Hsinchu, Taiwan. ³Institute of Atomic and Molecular Sciences, Academia Sinica, Taipei, Taiwan. ✉email: yplee@nycu.edu.tw

For the origin of life on earth it has long been presumed that prebiotic molecules were delivered from interstellar space through meteorites or comets or asteroids¹. The simplest amino acid, glycine $\text{NH}_2\text{CH}_2\text{C}(\text{O})\text{OH}$, is a key building block of proteins. Both glycine and methylamine, CH_3NH_2 , were detected in comets Wild 2 and 67P/Churyumov-Gerasimenko (67P/C-G); these observations provided strong evidence for a cosmic origin of amino acids on Earth^{2,3}, but the nature of the formation of glycine and other prebiotic molecules during the star-forming process remains unclear.

Several paths have been proposed for the formation of glycine according to theoretical calculations. Among them, the radical-radical reactions



appear to be more important than the ionic channels⁴. Garrod⁵ and Suzuki et al.⁶ employed a model consisting of processes in the gaseous phase, on grain surface, and in bulk ice in hot cores to indicate the key roles of reactions (1) and (2) in the formation of glycine on the grains. Sato et al. employed state-of-the-art DFT calculations and reported that reaction (1) is the most feasible route⁷; these authors proposed that the aminomethyl radical, $\bullet\text{CH}_2\text{NH}_2$, might be produced from successive hydrogenation of HCN or H abstraction from CH_3NH_2 by $\bullet\text{OH}$ or $\bullet\text{NH}_2$ ⁵⁻⁹. A similar theoretical chemical model involving NH_3 and $\bullet\text{HOCO}$ was also proposed to understand the main routes for the formation and decomposition of CH_3NH_2 ¹⁰.

Laboratory investigations to produce glycine from smaller precursors mimicking interstellar conditions have been extensive. UV photolysis and electron bombardment of various interstellar ice analogues such as $\text{CO}/\text{NH}_3/\text{H}_2\text{O}$ or $\text{H}_2\text{O}/\text{CH}_3\text{NH}_2/\text{CO}_2$ at low temperatures were demonstrated to yield glycine¹¹⁻¹⁸. Recently, Ioppolo et al.¹⁹ observed glycine formation from ices containing CH_3NH_2 , CO , O_2 , and atomic H under conditions similar to dark interstellar clouds; this result indicates that glycine can be formed with no need for energetic irradiation such as UV photons or cosmic rays, that is, during a much earlier star-formation stage than previously assumed. These authors proposed that glycine was produced via a barrierless radical-radical surface reaction (1), in which $\bullet\text{CH}_2\text{NH}_2$ was produced through H abstraction from CH_3NH_2 by $\bullet\text{OH}$ (produced from $\text{H} + \text{O}_2$) or H atom and $\bullet\text{HOCO}$ was produced via reaction between $\bullet\text{OH}$ and CO .

Even though the radical $\bullet\text{CH}_2\text{NH}_2$ plays a key role in the formation of glycine, its spectrum and mechanism of formation have yet to be directly identified. Bossa et al. reported that the isolation of this radical is difficult because of the reformation of CH_3NH_2 after the recombination of $\bullet\text{CH}_2\text{NH}_2$ with H atom; they consequently employed CO as an H-atom scavenger to diminish the recombination, but observed only formamide and N-methylformamide, not $\bullet\text{CH}_2\text{NH}_2$, after VUV (vacuum ultraviolet) irradiation of a $\text{CH}_3\text{NH}_2/\text{CO}$ binary ice mixture²⁰.

Here, we present direct experimental evidence, via IR spectra, of the formation of $\bullet\text{CH}_2\text{NH}_2$ and CH_2NH from the reaction of H atom with CH_3NH_2 via a H-abstraction tunneling reaction at low temperature, even in darkness. Furthermore, our experimental results showed a tight chemical connection between CH_3NH_2 and CH_2NH through dual H-abstraction and H-addition cycles.

Results and discussion

To perform H-atom reactions in the laboratory, we co-deposited Cl_2 , CH_3NH_2 , and *para*-hydrogen (*p*- H_2) at 3.2 K and irradiated the matrix with light at 365 nm from a light-emitting diode, followed by IR irradiation. The UV photolysis of Cl_2 at 365 nm

generated Cl atom, which is stable toward H_2 because the reaction $\text{Cl} + \text{H}_2 \rightarrow \text{HCl} + \text{H}$ is endothermic and has a large barrier²¹. The subsequent IR irradiation excites H_2 from $\nu=0$ to $\nu=1$ to overcome the energetic limitations so that the Cl atom reacts with H_2 ($\nu=1$) to form $\text{HCl} + \text{H}$. The H atom thus produced reacted with CH_3NH_2 during IR irradiation, but the reaction continued even when the matrix was maintained in darkness for a long period because the H atom could migrate slowly in the matrix via tunneling reactions to break and form neighboring H–H bonds (so-called quantum diffusion) to approach CH_3NH_2 and react via tunneling reactions. The efficient production of Cl from photolysis of Cl_2 in a low-temperature matrix requires a diminished cage effect, the production of H requires H_2 ($\nu=1$), and the migration of H in darkness requires quantum tunneling reaction; all these become possible only in quantum solid *p*- H_2 having associated unique properties^{22,23}.

Observation of methylamine radical ($\bullet\text{CH}_2\text{NH}_2$) and methylene imine (CH_2NH). The IR spectrum of a $\text{CH}_3\text{NH}_2/\text{Cl}_2/p\text{-H}_2$ (1/10/10000) matrix is shown in Supplementary Fig. 1a. The difference spectra after photolysis of the matrix at 365 nm for 30 min, subsequent IR irradiation for 90 min, maintenance of the matrix in darkness for 10 h, and secondary photolysis at 460 nm for 30 min are shown in Supplementary Fig. 1b–e, respectively. New features that appeared after IR irradiation, decreased by ~6% after being in darkness, and decreased by ~30% after secondary photolysis are indicated as group A, whereas those that appeared after IR irradiation, remained nearly constant after being in darkness, and increased by ~90% after secondary photolysis are indicated as group B. The difference spectrum after secondary photolysis at 460 nm (Supplementary Fig. 1e) in representative spectral regions is reproduced in Fig. 1b; lines in group A are pointing downward and those in group B are pointing upward, as indicated with color-coded arrows and labels.

The lines in group A at 3500.5, 3403.6, 3143.3, 3042.6, 1609.9, 1213.6, and 685.5 cm^{-1} agree well, in terms of wavenumbers and relative intensities, with the IR stick spectrum simulated for $\bullet\text{CH}_2\text{NH}_2$ (Fig. 1a) according to the scaled harmonic vibrational wavenumbers and IR intensities predicted with the B3LYP/aug-cc-pVTZ method; the scaling method is discussed in the Methods

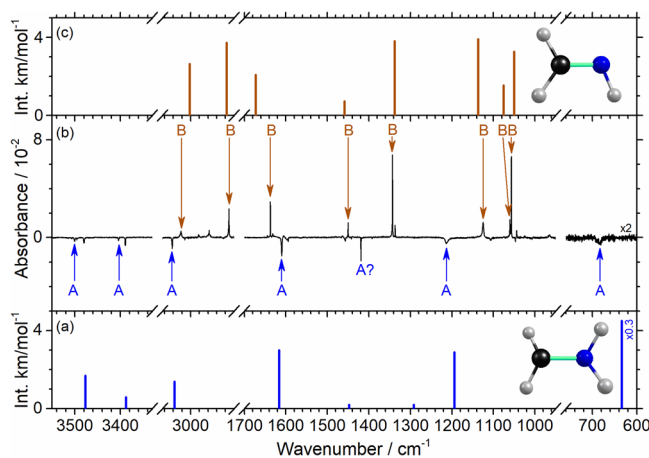


Fig. 1 Comparison of observed lines in groups A ($\bullet\text{CH}_2\text{NH}_2$) and B (CH_2NH) with theoretical calculations. **a** IR stick spectrum of aminomethyl radical $\bullet\text{CH}_2\text{NH}_2$. **b** IR difference spectrum after secondary photolysis at 460 nm of a UV/IR-irradiated $\text{CH}_3\text{NH}_2/\text{Cl}_2/p\text{-H}_2$ matrix after being maintained in darkness for 10 h; **c** IR stick spectrum of methylene imine CH_2NH . Both IR stick spectra in **a** and **c** were simulated according to scaled harmonic vibrational wavenumbers and IR intensities calculated with the B3LYP/aug-cc-pVTZ method.

Table 1 Comparison of observed wavenumbers and relative IR intensities of $\bullet\text{CH}_2\text{NH}_2$ in solid $p\text{-H}_2$ with their scaled harmonic vibrational wavenumbers and IR intensities predicted with the B3LYP/aug-cc-pVTZ method.

Mode	Sym.	$p\text{-H}_2$		B3LYP/aug-cc-pVTZ		Mode description ^c	$\Delta\nu$ ^e (cm^{-1})
		ν/cm^{-1}	Intensity ^a (%)	ν^b (cm^{-1})	Intensity (km mol^{-1})		
ν_1	A'	3403.6	20	3388	6	ν_s NH ₂	-15.6
ν_2	A'	3042.6	45	3037	14	ν_s CH ₂	-5.6
ν_3	A'	1609.9	100	1616	30	ρ NH ₂	6.1
ν_4	A'	1419.2 (?)	5	1448	2	δ CH ₂	—
ν_5	A'	1213.6	93	1194	29	ν CN/ ρ CH ₂	-19.6
ν_6	A'	685.5	^d	634	151	ω NH ₂	-51.5
ν_7	A'	—	—	562	128	ω CH ₂	—
ν_8	A''	3500.5	35	3477	17	ν_a NH ₂	-23.5
ν_9	A''	3143.3	11	3134	11	ν_a CH ₂	-9.3
ν_{10}	A''	—	—	1292	2	γ CH ₂ / γ NH ₂ / <i>ip-def</i>	—
ν_{11}	A''	—	—	913	1	γ NH ₂ / γ CH ₂	—
ν_{12}	A''	—	—	432	27	τ CH ₂ / τ NH ₂	—

^aIntegrated intensity relative to the most intense line at 1609.9 cm^{-1} (ν_3). ^bHarmonic vibrational wavenumber scaled with the linear equations $y = (0.9810 \pm 0.0126)x - (2.9 \pm 16.9)$ and $y = (0.8907 \pm 0.0084)x + (233.0 \pm 27.2)$ for regions below and above 2500 cm^{-1} , respectively. ^cApproximate mode description; ν : stretch, ρ : scissor, δ : bend, γ : rock, ω : wag, *def*: deformation, τ : twist, *ip*: in-plane, subscript *a*: antisymmetric, and subscript *s*, symmetric. ^dIntense absorption of solid $p\text{-H}_2$ near 710 cm^{-1} interfered with the intensity measurement. ^eDeviation $\Delta\nu = \nu_{\text{calculated}} - \nu_{\text{experimental}}$.

section. To understand the perturbations of H_2 on the IR spectrum of $\bullet\text{CH}_2\text{NH}_2$, we performed calculations also on $\bullet\text{CH}_2\text{NH}_2$ surrounded by eighteen H_2 molecules, either in a hexagonal-closed pack (*hcp*) lattice or randomly (free optimization). The resultant vibrational wavenumbers and IR intensities are compared in Supplementary Table 1 and the simulated IR stick spectra of $\bullet\text{CH}_2\text{NH}_2$ are presented in Supplementary Fig. 2 to compare with calculations for gaseous $\bullet\text{CH}_2\text{NH}_2$ and experiments. The perturbation by H_2 is small (with average absolute deviations 8.8 ± 6.0 and $14.8 \pm 8.5\text{ cm}^{-1}$ from the gaseous phase; listed errors represent one standard deviation in fitting) and within calculation errors. This is in line with the fact that observed IR spectra of matrix-isolated species typically showed $<1\%$ matrix shifts so that comparison of observed vibrational wavenumbers with predictions of gaseous species was generally performed. The observed lines in group A agree poorly with stick IR spectra of other possible products, as shown in Supplementary Fig. 3.

The symmetric and antisymmetric NH₂-stretching modes of $\bullet\text{CH}_2\text{NH}_2$ predicted near 3388 and 3477 cm^{-1} were observed at 3403.6 and 3500.5 cm^{-1} , respectively. The symmetric and antisymmetric CH₂-stretching modes predicted near 3037 and 3134 cm^{-1} were observed at 3042.6 and 3143.3 cm^{-1} , respectively. The NH₂-scissoring mode predicted at 1616 cm^{-1} agrees with the observed feature at 1609.9 cm^{-1} . The CN-stretching mode coupled with CH₂-scissoring, predicted near 1194 cm^{-1} , was observed at 1213.6 cm^{-1} . The most intense line predicted for the NH₂-wagging mode at 634 cm^{-1} was observed at 685.5 cm^{-1} . Experiments and calculations are compared in Table 1. The observed features in group A can hence be clearly assigned to $\bullet\text{CH}_2\text{NH}_2$. The average absolute deviation between experiment and prediction is $18.7 \pm 15.2\text{ cm}^{-1}$ ($1.06 \pm 0.8\%$) for $\bullet\text{CH}_2\text{NH}_2$. The large deviation for ν_6 (CH₂ wag) is typical for this mode because of the inadequacy in describing the double-well potential experienced by N atom, similar to NH₃. All lines of $\bullet\text{CH}_2\text{NH}_2$ located in our detection spectral range with predicted IR intensity greater than 6 km mol^{-1} were observed; predicted lines near 1448 and 1292 cm^{-1} have intensity $\sim 2\text{ km mol}^{-1}$ too small to be observed.

The lines in group B at 3260.2 , 3022.4 , 2912.1 , 1637.4 , 1450.2 , 1343.3 , 1125.1 , 1060.3 , and 1056.9 cm^{-1} are readily assigned to methylene imine CH₂NH, of which the IR spectrum in solid $p\text{-H}_2$

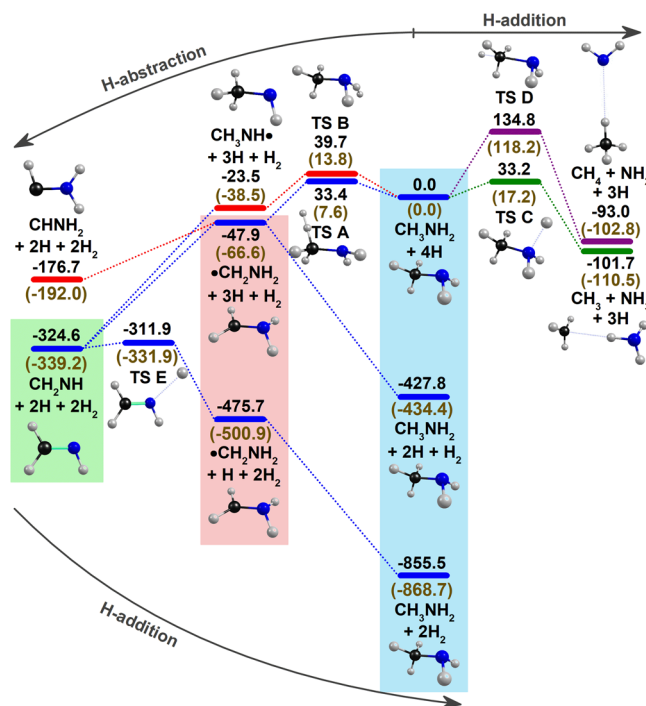


Fig. 2 Potential-energy scheme of H-addition and H-abstraction of CH_3NH_2 calculated with the CCSD(T)/aug-cc-pVTZ//B3LYP/aug-cc-pVTZ method. Energies corrected for zero-point vibrational energy (ZPVE) are in kJ mol^{-1} ; those calculated with the B3LYP/aug-cc-pVTZ methods are listed in parentheses for comparison.

was recorded by Ruzi and Anderson on photodissociation at 193 nm of *N*-methylformamide in solid $p\text{-H}_2$ ²⁴. The observed vibrational wavenumbers and relative intensities also agree with those predicted for CH₂NH, as shown in Fig. 1c. A comparison of experiments with theoretical calculations is presented in Supplementary Table 2.

To explore the possible products of reaction $\text{H} + \text{CH}_3\text{NH}_2$, we performed quantum-chemical calculations with the CCSD(T)/aug-cc-pVTZ//B3LYP/aug-cc-pVTZ method. The potential-energy scheme for H-abstraction (left side) and H-addition (right

side) is shown in Fig. 2; to be self-consistent in terms of energy and species involved, we included all H atoms and H₂ involved in this reaction network. The first H-abstraction from either moiety CH₃ or NH₂ of CH₃NH₂ (light blue background) results in the formation of •CH₂NH₂ (pink background) or CH₃NH•, respectively; abstraction on the CH₃ site has a smaller barrier and is more exothermic. The H-addition to either moiety NH₂ or CH₃ of CH₃NH₂ results in the rupture of the C–N bond to form CH₃ + NH₃ (the most exothermic) or CH₄ + NH₂ (involving the largest barrier). Both radicals can proceed with further H-abstraction without barrier to form closed-shell methylene imine CH₂NH (light green background). The H-addition to •CH₂NH₂ to reproduce CH₃NH₂ is barrierless, and that to CH₂NH to form •CH₂NH₂ has a small barrier (~13 kJ mol⁻¹).

The observation of •CH₂NH₂ (group A) and CH₂NH (group B) agrees with the predicted minimal paths for consecutive H-abstraction of CH₃NH₂. The H-abstraction of •CH₂NH₂ to form CH₂NH is barrierless, whereas that of CH₃NH₂ to form •CH₂NH₂ has barrier ~33 kJ mol⁻¹, small enough for the tunneling reaction to occur even at 3.2 K. Our previous observations of H-abstraction of methanol²⁵, formamide²⁶, methyl formate²⁷, acetamide²⁸, acetic acid²⁹, and glycine³⁰ by H atoms showed predicted barriers of 36, 26, 41, 41, 43, and 29 kJ mol⁻¹, respectively. Although the calculations showed that H abstraction on the amino hydrogen to form CH₃NH• has a barrier ~40 kJ mol⁻¹, we did not observe CH₃NH•, which can be readily identified at 3241.5, 2828.9, 2795.5, 1365.8, 1025.2 cm⁻¹ in solid *p*-H₂ as reported by Ruzi and Anderson²⁴.

The destruction of •CH₂NH₂ to form CH₂NH upon irradiation at 460 nm also agrees with the TD-B3LYP/aug-cc-pVTZ calculations showing an absorption band near 450 nm corresponding to HOMO (α) → LUMO (α) for •CH₂NH₂ (Supplementary Figs. 4 and 5 and Supplementary Table 3), but no absorption for CH₃NH₂ at wavelength greater than 250 nm. We observed also the formation of a small proportion of NH₃ (~8% of •CH₂NH₂), indicating that H addition to CH₃NH₂ produced CH₃ + NH₃. We observed also CH₃Cl, likely produced from the reaction of CH₃ with Cl.

Isotopic Substitution reaction. We performed also experiments on partially deuterated methyl amine, CD₃NH₂. The representative spectra at various stages are depicted in Supplementary Fig. 6. The IR difference spectrum on secondary photolysis at 460 nm of the UV/IR-irradiated matrix after being maintained in darkness for 10 h is compared with IR stick spectra predicted for •CD₂NH₂ and CD₂NH in Supplementary Fig. 7. Lines in group A' match with IR lines predicted for •CD₂NH₂. Similarly, lines in group B' match with those predicted for CD₂NH. In addition to lines in group A' and group B', we observed lines at 2125.2, 996.2, 937.6, 838.7, and 769.7 cm⁻¹, denoted group C', that can be assigned to CD₂HNNH₂, as presented in Supplementary Fig. 8. This observation confirms that H addition to •CD₂NH₂ produced CD₂HNNH₂. A comparison of experimental results and calculations for •CD₂NH₂, CD₂NH, and CD₂HNNH₂ is listed in Supplementary Tables 4–6. This isotopic experiment provides not only spectral confirmation of •CH₂NH₂ and CH₂NH, but also direct evidence of the conversion of •CH₂NH₂ back to CH₃NH₂ by H-addition, consistent with the report by Oba et al. that H–D substitution of solid CH₃NH₂ (and its isotopologues) is more rapid in the CH₃ moiety than in the NH₂ moiety when CH₃NH₂ reacts with H or D atoms under astrophysically relevant conditions³¹. Although we performed no experiment on CD₃ND₂ to confirm that H + CD₂ND → •CD₂NDH occurred, we expect this reaction to occur because of a small barrier.

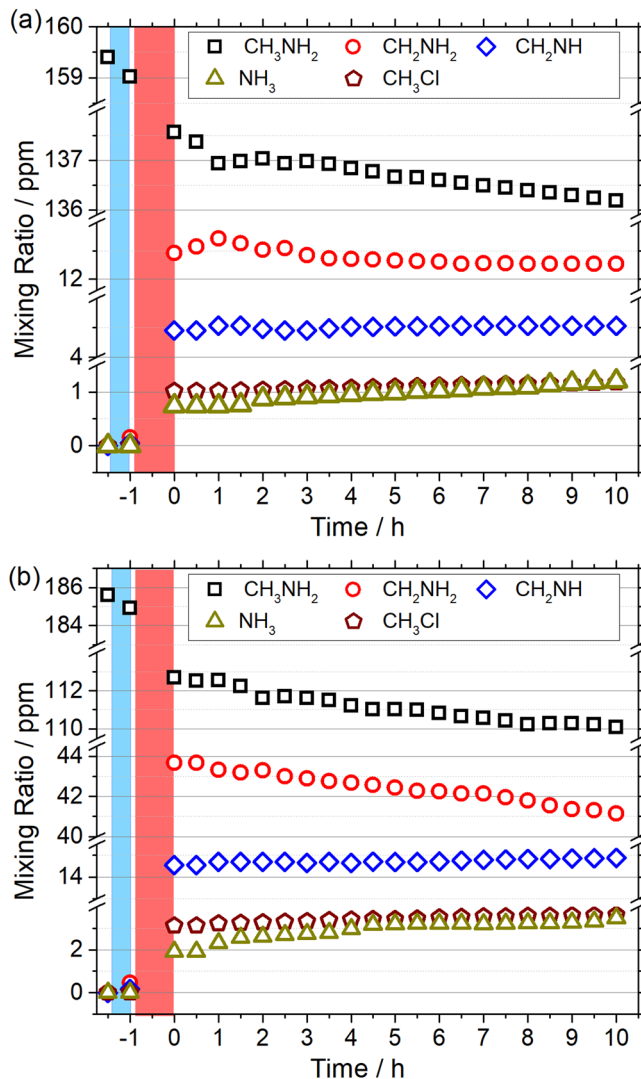


Fig. 3 Temporal evolution of mixing ratios of CH₃NH₂, •CH₂NH₂, CH₂NH, NH₃, and CH₃Cl upon UV and IR irradiation of a CH₃NH₂/Cl₂/*p*-H₂ matrix, followed by maintenance in darkness. **a** [H]₀/[CH₃NH₂]₀ ≈ 2.1 and [CH₃NH₂]₀ = 159 ppm, **b** [H]₀/[CH₃NH₂]₀ ≈ 7.2 and [CH₃NH₂]₀ = 186 ppm. The regions shaded with blue and red correspond to periods of UV and IR irradiation, respectively.

Temporal profiles and reaction mechanism. The temporal evolution of the mixing ratios of each species is presented in Fig. 3 for two conditions with [H]₀/[CH₃NH₂]₀ ≈ 2.1 ([CH₃NH₂]₀ ≈ 159 ppm) and [H]₀/[CH₃NH₂]₀ ≈ 7.2 ([CH₃NH₂]₀ ≈ 186 ppm); details are discussed in Supplementary Note 1. •CH₂NH₂ was the dominant product, followed by CH₂NH. In the H-deficient experiment, we observed an initial increase of •CH₂NH₂, followed by a decrease to reach a constant mixing ratio, consistent with the two-step mechanism for the formation from the first H abstraction of CH₃NH₂ and the destruction due to the second H abstraction; the *anti*-correlation between the mixing ratios of CH₃NH₂ and •CH₂NH₂ was clearly visible. In the H-rich experiment, •CH₂NH₂ and CH₂NH increased significantly upon IR irradiation, and •CH₂NH₂ continuously decreased in darkness, indicating more significant H abstraction of •CH₂NH₂ due to the presence of more H atoms.

The observation of consecutive H abstraction of CH₃NH₂ to form •CH₂NH₂ and CH₂NH, and their H-addition to reform

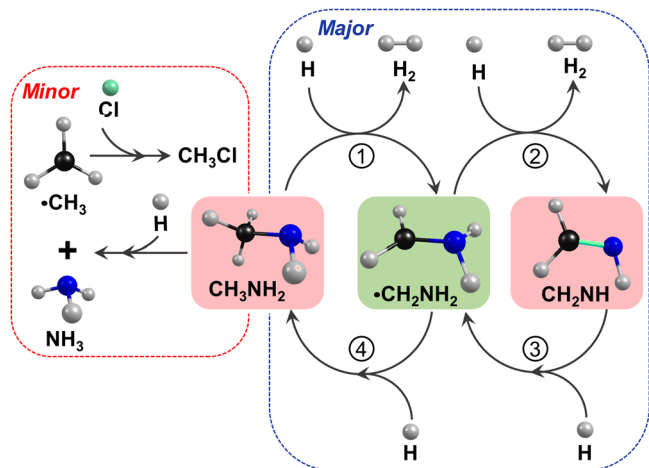


Fig. 4 Dual-cycle mechanism of H-abstraction and H-addition reactions connecting CH_3NH_2 , $\bullet\text{CH}_2\text{NH}_2$, and CH_2NH and the formation of CH_3 and NH_3 . The area on the right with blue dotted boundary represents the major dual-cycle channels connecting CH_3NH_2 , $\bullet\text{CH}_2\text{NH}_2$, and CH_2NH with two sets of H-abstraction and H-addition reactions. The area on the left with red dotted boundary represents minor reactions channels of the decomposition of CH_3NH_2 to form CH_3 and NH_3 upon H addition).

CH_3NH_2 and $\bullet\text{CH}_2\text{NH}_2$, respectively, connects CH_3NH_2 , $\bullet\text{CH}_2\text{NH}_2$, and CH_2NH via a dual-cycle mechanism shown in Fig. 4, similar to that among formamide HC(O)NH_2 , H_2NCO and HNCO ²⁶. The first H-abstraction channel (reaction 1) depicted in Fig. 4 was reported by Garrod⁵ and Suzuki⁶ in their theoretical models. Hydrogenation of solid HCN and CH_2NH at low temperature conducted by Theule et al.³² resulted in the formation of CH_3NH_2 directly, indicating the presence of two consecutive H addition (reactions 3 and 4), even though $\bullet\text{CH}_2\text{NH}_2$ was not observed directly. In the present study, all guest molecules are well isolated in solid *p*- H_2 at low temperature so that free radicals such as $\bullet\text{CH}_2\text{NH}_2$ have much better chance to be trapped and maintained. Furthermore, because the hydrogenation experiments by Theule et al.³² were carried out by hydrogen bombardment, $\bullet\text{CH}_2\text{NH}_2$ is expected to react readily with a second hydrogen atom to form the end product CH_3NH_2 . Our observations of the formation of $\bullet\text{CH}_2\text{NH}_2$ and CH_2NH in darkness and the formation of CD_2HNNH_2 from H reactions with CD_3NH_2 further support the dual-cycle mechanism.

We understand that our experimental conditions do not mimic the ISM conditions closely, so our results cannot be applied directly to the reactions in the ISM. For example, in the case of water ice environments, the interaction between water and the guest species might be stronger so that the stability and reactivity of radicals are different from the gaseous phase, as demonstrated by the simulations of radical-radical reactions on icy surfaces by Enrique-Romero et al.³³ Nevertheless, our results clearly indicate that reaction of H with methylamine CH_3NH_2 produces $\bullet\text{CH}_2\text{NH}_2$, an important radical precursor for the formation of glycine, directly supporting the mechanism, reaction (1), proposed by Ioppolo et al.¹⁹ for the formation of glycine under conditions similar to dark interstellar clouds with no need for UV irradiation or cosmic rays. The mobility of chemical reactants in the bulk ice is assumed through a swapping mechanism that was supported by laboratory work^{34,35} and theoretical investigations⁵; this mechanism likely brings H atom and CH_3NH_2 in close proximity to react.

Conclusions

The IR spectrum of $\bullet\text{CH}_2\text{NH}_2$ is previously unreported; it provides a unique tool to probe this important intermediate, a precursor of glycine. We showed also the order of the consecutive H abstraction of CH_3NH_2 to be on the CH_3 moiety first (to produce $\bullet\text{CH}_2\text{NH}_2$), followed by the NH_2 moiety (to produce CH_2NH); the presence of the back reaction (H addition to radicals) was confirmed in experiments of $\text{H} + \text{CD}_3\text{NH}_2$ to produce CD_2HNNH_2 . This dual-cycle mechanism provides an explanation that CH_2NH and CH_3NH_2 might be chemically connected. CH_2NH was also considered to be a precursor of glycine via reactions with $\text{CO} + \text{H}_2\text{O}$ or $\text{CO}_2 + \text{H}_2$ in hot core or cold molecular clouds^{36–38}.

Methods

Experimental details. A description on the IR absorption matrix-isolation system using *p*- H_2 as a matrix host is available elsewhere^{22,39,40}. A nickel-coated copper plate at 3.2 K served as a cold substrate for matrix samples and also for reflection absorption spectra. A closed-cycle helium refrigerator system was used to cool the substrate. A gaseous mixture of $\text{CH}_3\text{NH}_2/\text{Cl}_2/p\text{-H}_2$ (1/10/10000) was deposited, typically over a period of 9 h at a flow rate ~ 7 STP $\text{cm}^3 \text{min}^{-1}$ (STP indicates standard temperature 273 K and pressure 760 torr). The photolysis of Cl_2 in the matrix at 365 nm (light-emitting diode, 5 W) produced Cl atoms; subsequent IR irradiation (unfiltered external SiC source) promoted the reaction $\text{Cl} + \text{H}_2$ ($\nu = 1$) $\rightarrow \text{H} + \text{HCl}$, resulting in the generation of H atoms. The matrix was maintained in darkness for 10 h to study H-tunneling reactions and was further photolyzed with light at 460 nm to distinguish lines of each species. To generate *p*- H_2 , normal H_2 (99.9999%) was passed through a trap at 77 K before entering a converter containing an iron(III)-oxide catalyst cooled to 12.9 K with a closed-cycle helium refrigerator. Methylamine (CH_3NH_2 , Sigma-Aldrich, purity $\geq 99\%$), having vapor pressure ~ 1400 Torr at 293 K, was used to prepare a gaseous mixture $\text{CH}_3\text{NH}_2/p\text{-H}_2$ (1/10000). Methylamine- d_3 (CD_3NH_2 , Cambridge Isotope Laboratories, $\geq 98\%$ isotopic purity) was used for isotopic experiments. A Fourier-transform infrared (FTIR) spectrometer equipped with KBr beam splitter and HgCdTe detector at 77 K was used to record IR absorption spectra covering a spectral range 600–4000 cm^{-1} . A total of 200 interferometric scans at a resolution of 0.25 cm^{-1} were typically recorded at each stage of the experiment.

Quantum-chemical calculations. Geometry optimizations and vibrational analyses (wavenumbers and IR intensities) were calculated with the Gaussian16 program package⁴¹. Density-functional theory calculations were performed using B3LYP functionals⁴² and standard Dunning's correlation-consistent basis set augmented with diffuse functions, aug-cc-pVTZ⁴³. Furthermore, calculations on single-point electronic energies with the method coupled cluster with single and double and perturbative triple excitations, CCSD(T)⁴⁴, were performed on geometries obtained with the B3LYP/aug-cc-pVTZ method; zero-point vibrational energies (ZPVE) were corrected according to the harmonic vibrational wavenumbers calculated with the B3LYP method. Both harmonic and anharmonic vibrational wavenumbers were calculated with the B3LYP/aug-cc-pVTZ method. To obtain scaled harmonic vibrational wavenumbers, plots of observed wavenumbers against calculated harmonic vibrational wavenumbers were employed for two separate regions. Two linear equations, $y = (0.9810 \pm 0.0126)x - (2.9 \pm 16.9)$ and $y = (0.8907 \pm 0.0084)x + (233.0 \pm 27.2)$, were derived for regions 800–1700 and 2900–3600 cm^{-1} , respectively; y is the observed wavenumber and x is the calculated harmonic vibrational wavenumber. The average absolute deviation is $5.1 \pm 3.8 \text{ cm}^{-1}$ between experiments and scaled harmonic vibrational wavenumbers of CH_3NH_2 and $16.4 \pm 22.7 \text{ cm}^{-1}$ between experiments and anharmonic vibrational wavenumbers of CH_3NH_2 . The same equations were employed to scale harmonic vibrational wavenumbers of all species considered in this work.

Data availability

The data that support the plots within this paper and other findings of this study are available from the corresponding author upon reasonable request.

Received: 5 January 2022; Accepted: 26 April 2022;
Published online: 12 May 2022

References

1. Krishnamurthy, R. & Hud, N. V. Introduction: chemical evolution and the origins of life. *Chem. Rev.* **120**, 4613–4615 (2020).

- Elsila, J. E., Glavin, D. P. & Dworkin, J. P. Cometary glycine detected in samples returned by Stardust. *Meteorit. Planet. Sci.* **44**, 1323–1330 (2009).
- Altwegg, K. et al. Prebiotic chemicals-amino acid and phosphorus-in the coma of comet 67P/Churyumov-Gerasimenko. *Sci. Adv.* **2**, e1600285 (2016).
- Pilling, S., Baptista, L., Boechat-Roberty, H. M. & Andrade, D. P. P. Formation routes of interstellar glycine involving carboxylic acids: possible favoritism between gas and solid phase. *Astrobiology* **11**, 883–893 (2011).
- Garrod, R. T. A three-phase chemical model of hot cores: the formation of glycine. *Astrophys. J.* **765**, 60 (2013).
- Suzuki, T. et al. An expanded gas-grain model for interstellar glycine. *Astrophys. J.* **863**, 51 (2018).
- Sato, A. et al. First-principles study of the formation of glycine-producing radicals from common interstellar species. *Mol. Astrophys.* **10**, 11–19 (2018).
- Woon, D. E. Pathways to glycine and other amino acids in ultraviolet-irradiated astrophysical ices determined via quantum chemical modelling. *Astrophys. J.* **571**, L177–L180 (2002).
- Singh, A., Shivani, M. A. & Tandon, P. Quantum chemical analysis for the formation of glycine in the interstellar medium. *Res. Astron. Astrophys.* **13**, 912–920 (2013).
- de Jesus, D. N. et al. Chemical mechanism for decomposition of CH_3NH_2 and implications to interstellar glycine. *Mon. Not. Roy. Astron. Soc.* **501**, 1202–1214 (2021).
- Briggs, R. et al. Comet Halley as an aggregate of interstellar dust and further evidence for the photochemical formation of organics in the interstellar-Medium. *Orig. Life Evol. Biosph.* **22**, 287–307 (1992).
- Caro, G. M. M. et al. Amino acids from ultraviolet irradiation of interstellar ice analogues. *Nature* **416**, 403–406 (2002).
- Bernstein, M. P., Dworkin, J. P., Sandford, S. A., Cooper, G. W. & Allamandola, L. J. Racemic amino acids from the ultraviolet photolysis of interstellar ice analogues. *Nature* **416**, 401–403 (2002).
- Elsila, J. E., Dworkin, J. P., Bernstein, M. P., Martin, M. P. & Sandford, S. A. Mechanisms of amino acid formation in interstellar ice analogs. *Astrophys. J.* **660**, 911–918 (2007).
- Lee, C. W., Kim, J. K., Moon, E. S., Minh, Y. C. & Kang, H. Formation of glycine on ultraviolet-irradiated interstellar ice-analog films and implications for interstellar amino acids. *Astrophys. J.* **697**, 428–435 (2009).
- Sugahara, H. et al. Molecular and isotopic compositions of nitrogen-containing organic molecules formed during UV-irradiation of simulated interstellar ice. *Geochem. J.* **53**, 5–20 (2019).
- Holtom, P. D., Bennett, C. J., Osamura, Y., Mason, N. J. & Kaiser, R. I. A combined experimental and theoretical study on the formation of the amino acid glycine ($\text{NH}_2\text{CH}_2\text{COOH}$) and its isomer (CH_2NHCOOH) in extraterrestrial ices. *Astrophys. J.* **626**, 940–952 (2005).
- Esmaili, S., Bass, A. D., Cloutier, P., Sanche, L. & Huels, M. A. Glycine formation in CO_2 : CH_4 : NH_3 ices induced by 0–70 eV electrons. *J. Chem. Phys.* **148**, 164702 (2018).
- Ioppolo, S. et al. A non-energetic mechanism for glycine formation in the interstellar medium. *Nat. Astron.* **5**, 197–205 (2021).
- Bossa, J. B. et al. Solid-state methylamine VUV irradiation study using carbon monoxide as an H radical scavenger. *Aust. J. Chem.* **65**, 129–137 (2012).
- Raston, P. L., Kettwich, S. C. & Anderson, D. T. Kinetic studies of the infrared-induced reaction between atomic chlorine and solid parahydrogen. *J. Mol. Spectrosc.* **310**, 72–83 (2015).
- Tsuge, M., Tseng, C. Y. & Lee, Y.-P. Spectroscopy of prospective interstellar ions and radicals isolated in *para*-hydrogen matrices. *Phys. Chem. Chem. Phys.* **20**, 5344–5358 (2018).
- Tsuge, M. & Lee, Y.-P. Spectroscopy of molecules confined in solid *Para*-hydrogen. *Mol. Laser Spectrosc.* **2**, 167–215 (2020).
- Ruzi, M. & Anderson, D. T. Photodissociation of N-methylformamide isolated in solid parahydrogen. *J. Chem. Phys.* **137**, 194313 (2012).
- Haupa, K. A., Johnson, B. A., Sibert, E. L. & Lee, Y.-P. Infrared absorption spectra of partially deuterated methoxy radicals CH_2DO and CHD_2O isolated in solid *para*-hydrogen. *J. Chem. Phys.* **147**, 154305 (2017).
- Haupa, K. A., Tarczay, G. & Lee, Y.-P. Hydrogen abstraction/addition tunneling reactions elucidate the interstellar $\text{H}_2\text{NCHO}/\text{HNCO}$ ratio and H_2 formation. *J. Am. Chem. Soc.* **141**, 11614–11620 (2019).
- Haupa, K. A., Strom, A. I., Anderson, D. T. & Lee, Y.-P. Hydrogen-atom tunneling reactions with methyl formate in solid *para*-hydrogen: infrared spectra of the methoxy carbonyl [$\bullet\text{C}(\text{O})\text{OCH}_3$] and formyloxy methyl [$\text{HC}(\text{O})\text{OCH}_2\bullet$] radicals. *J. Chem. Phys.* **151**, 234302 (2019).
- Haupa, K. A., Ong, W. S. & Lee, Y.-P. Hydrogen abstraction in astrochemistry: formation of $\bullet\text{CH}_2\text{CONH}_2$ in the reaction of H atom with acetamide (CH_3CONH_2) and photolysis of $\bullet\text{CH}_2\text{CONH}_2$ to form ketene (CH_2CO) in solid *para*-hydrogen. *Phys. Chem. Chem. Phys.* **22**, 6192–6201 (2020).
- Joshi, P. R., How, K. C. Y. & Lee, Y.-P. Hydrogen abstraction of acetic acid by hydrogen atom to form carboxymethyl radical $\bullet\text{CH}_2\text{C}(\text{O})\text{OH}$ in solid *para*-hydrogen and its implication in astrochemistry. *ACS Earth Space Chem.* **5**, 106–117 (2021).
- Schneiker, A. et al. Non-energetic, low-temperature formation of Ca-glycyl radical, a potential interstellar precursor of natural amino acids. *J. Phys. Chem. Lett.* **12**, 6744–6751 (2021).
- Oba, Y., Chigai, T., Osamura, Y., Watanabe, N. & Kouchi, A. Hydrogen isotopic substitution of solid methylamine through atomic surface reactions at low temperatures: a potential contribution to the D/H ratio of methylamine in molecular clouds. *Meteorit. Planet. Sci.* **49**, 117–132 (2014).
- Theule, P. et al. Hydrogenation of solid hydrogen cyanide HCN and methanimine CH_2NH at low temperature. *Astron. Astrophys.* **534**, A64 (2011).
- Enrique-Romero, J. et al. Quantum mechanical simulations of the radical-radical chemistry on icy surfaces. *Astrophys. J. Suppl. Ser.* **259**, 39 (2022).
- Oberg, K. I., Fayolle, E. C., Cuppen, H. M., van Dishoeck, E. F. & Linnartz, H. Quantification of segregation dynamics in ice mixtures. *Astron. Astrophys.* **505**, 183–194 (2009).
- Fayolle, E. C., Oberg, K. I., Cuppen, H. M., Visser, R. & Linnartz, H. Laboratory $\text{H}_2\text{O}:\text{CO}_2$ ice desorption data: entrapment dependencies and its parameterization with an extended three-phase model. *Astron. Astrophys.* **529**, A74 (2011).
- Wang, L.-P. et al. Discovering chemistry with an ab initio nanoreactor. *Nat. Chem.* **6**, 1044–1048 (2014).
- Nhlabatsi, Z. P., Bhasi, P. & Sitha, S. Possible interstellar formation of glycine through a concerted mechanism: a computational study on the reaction of $\text{CH}_2 = \text{NH}$, CO_2 and H_2 . *Phys. Chem. Chem. Phys.* **18**, 20109–20117 (2016).
- Nhlabatsi, Z. P., Bhasi, P. & Sitha, S. Possible interstellar formation of glycine from the reaction of $\text{CH}_2 = \text{NH}$, CO and H_2O : catalysis by extra water molecules through the hydrogen relay transport. *Phys. Chem. Chem. Phys.* **18**, 375–381 (2016).
- Golec, B., Das, P., Bahou, M. & Lee, Y.-P. Infrared spectra of the 1-pyridinium ($\text{C}_5\text{H}_5\text{NH}^+$) cation and pyridinyl ($\text{C}_5\text{H}_5\text{NH}$ and $4\text{-C}_5\text{H}_6\text{N}$) radicals isolated in solid *para*-hydrogen. *J. Phys. Chem. A* **117**, 13680–13690 (2013).
- Bahou, M., Das, P., Lee, Y. F., Wu, Y. J. & Lee, Y.-P. Infrared spectra of free radicals and protonated species produced in *para*-hydrogen matrices. *Phys. Chem. Chem. Phys.* **16**, 2200–2210 (2014).
- Frisch, M. J. et al. Gaussian 16 (revision B.01), Inc., Wallingford CT USA, 2016.
- Boys, S. F. & Bernardi, F. The calculation of small molecular interactions by the differences of separate total energies. Some procedures with reduced errors. *Mol. Phys.* **19**, 553–566 (1970).
- Dunning, T. H. Gaussian basis sets for use in correlated molecular calculations. I. The atom boron through neon and hydrogen. *J. Chem. Phys.* **90**, 1007–1023 (1989).
- Purvis, G. D. & Bartlett, R. J. A full couple-cluster singles and doubles model: the inclusion of disconnected triples. *J. Chem. Phys.* **76**, 1910–1918 (1982).

Acknowledgements

This work was supported by Ministry of Science and Technology, Taiwan (Grants nos. MOST 110-2639-M-A49-001-ASP and 110-2634-F-009-026) and the Center for Emergent Functional Matter Science of National Chiao Tung University from The Featured Areas Research Center Program within the framework of the Higher Education Sprout Project by the Ministry of Education (MOE) in Taiwan. The National Center for High-Performance Computation provided computer time.

Author contributions

P.R.J. performed all computations, experiments, and initial analysis and wrote an initial draft; Y.-P.L. formulated and administered the research project, acquired the funding, finalized the analysis, and wrote the manuscript with contributions from P.R.J.

Competing interests

The authors declare no competing interests.

Additional information

Supplementary information The online version contains supplementary material available at <https://doi.org/10.1038/s42004-022-00677-5>.

Correspondence and requests for materials should be addressed to Yuan-Pern Lee.

Peer review information *Communications Chemistry* thanks Nadia Balucani and the other, anonymous, reviewer(s) for their contribution to the peer review of this work. Peer reviewer reports are available.

Reprints and permission information is available at <http://www.nature.com/reprints>

Publisher's note Springer Nature remains neutral with regard to jurisdictional claims in published maps and institutional affiliations.



Open Access This article is licensed under a Creative Commons Attribution 4.0 International License, which permits use, sharing, adaptation, distribution and reproduction in any medium or format, as long as you give appropriate credit to the original author(s) and the source, provide a link to the Creative Commons license, and indicate if changes were made. The images or other third party material in this article are included in the article's Creative Commons license, unless indicated otherwise in a credit line to the material. If material is not included in the article's Creative Commons license and your intended use is not permitted by statutory regulation or exceeds the permitted use, you will need to obtain permission directly from the copyright holder. To view a copy of this license, visit <http://creativecommons.org/licenses/by/4.0/>.

© The Author(s) 2022